Decoupled Circular-Polarized Dual-Head Volume Coil Pair for Studying Two Interacting Human Brains with Dyadic fMRI

Ray F. Lee,* W. Dai, and J. Jones

A major function of the human brain is to mediate interactions with other people. Until recently, studying social interactions as they occur within the brain was not possible due to the lack of measurable methods to observe two interacting minds simultaneously. We have developed a novel MRI dual-head volume coil pair that can scan two subjects' brains simultaneously while the subjects are socially interacting in one MRI scanner. The feasibility of using this coil for dyadic functional MRI (fMRI) study has been successfully demonstrated for the first time. Meanwhile, an innovative robust scheme for decoupling two circular-polarized coils (not surface coils) is introduced in theory and validated in practice in the coil technology development. Magn Reson Med 68:1087–1096, 2012. © 2011 Wiley Periodicals, Inc.

Key words: dual-head volume coil; DHVC; dyadic fMRI; dfMRI; circular-polarized decoupling; brain interaction; geometric decoupling; decoupling interface; directional coupler

A major function of the human brain is to mediate interactions with other people, such as interpersonal communication and physical contact. Understanding such dynamic interactions between two minds is essential for characterizing human social behavior. Until recently, studying the neural mechanisms that underlie social interaction was not possible due to the lack of measurable methods to observe two interacting minds simultaneously. Fortunately, research in this field has progressed in recent years with the usage of modern imaging modalities such as MRI and EEG (1–6). "Hyperscanning," a technique developed by Montague et al., uses the internet to connect and synchronize two MRI scanners while two subjects are scanned and play a simple deception game (7). Redcay et al. investigated "face-to-face interaction" in fMRI by providing subjects with a live visual feed of the experimenter as their stimulus (8). However, to avoid the indirect effects present in past research and achieve observation of the direct interaction between two brains, we have developed a novel MRI dual-head volume coil (DHVC) that allows for the acquisition of dyadic fMRI (dfMRI) signals from two subjects' brains while the subjects are in close proximity of one another inside a single scanner. This technology grants the investigation and understanding of dyadic social interactions, including physical contact, which is not possible with any other fMRI technique.

Although there are many technical challenges for dfMRI in a current commercial MRI scanner, the most essential enabling technology is to build a DHVC pair, which can provide a homogeneous radio frequency (RF) transmit/receive field over two brains while keeping the SAR level in check. In our approach, by placing two birdcages (9,10) side-by-side, the critical technical challenge is to decouple two strongly coupled circular-polarized (CP) RF volume resonators. This issue has not properly been addressed in both theory and practice thus far. In this work, we fully resolved this issue by combining both the even-odd mode theory (11) and the decoupling interface method (12): First, we geometrically adjusted two birdcages to form even- and odd-modes where the even-mode magnetic fields are intrinsically decoupling; Second, the tightly coupled odd-mode magnetic fields are then decoupled by a properly designed directional coupler. Together, they yield a robust and passive isolation between two CP coils, which provides sufficient (−40 to −60 dB) decoupling for high-power transmit array.

A prototype DHVC was built and integrated into a commercial MRI scanner. The dfMRI studies of more than 20 in vivo human brain pairs were successfully conducted by using this DHVC, successfully revealing the BOLD effect of the direct interaction between two human brains for the first time.

THEORY AND METHOD

Coil Structure and Design

The DHVC consists of two birdcages placed side-by-side inside the magnet bore, as shown in Fig. 1. For the purpose of demonstrating feasibility, we limited our essential design goals to three areas: (i) First, to optimize the spatial dimensions of the coil pair so that they not only fit two human heads but also allow their two homogeneous RF field B_1 regions to be within the homogeneous static magnetic field B_0 region; (ii) Second, the two subjects would have complete facial view of each other when they are inside the coil pair; (iii) Third, and the main focus of this work, to robustly decouple two CP volume transmit/receive coils with reactance-only passive circuits, which, unlike decoupling two surface coils, has not been reported in literature so far.

Princeton Neuroscience Institute, Princeton University, Princeton, New Jersey, USA.

*Correspondence to: Ray F. Lee, PhD, Princeton Neuroscience Institute, Princeton University, Green Hall 0-N-14, Princeton, NJ 08544.
E-mail: raylee@princeton.edu

Received 9 August 2011; revised 24 October 2011; accepted 12 November 2011.

DOI 10.1002/mrm.23313
Published online 28 December 2011 in Wiley Online Library (wileyonlinelibrary.com).

FIG. 1. The (**a**) is a conceptual drawing of DHVC inside bore. The (**b**) is the photo of two birdcages whose rungs are positioned so that their composite field forms even- and odd-mode. The (**c**) is the frontal view of the schematic of the two birdcages in (b), where even and odd port are at 0° and 90°, and the four rungs are at 45°, 135°, 225°, and 315°. [Color figure can be viewed in the online issue, which is available at wileyonlinelibrary.com.]

The standard inner bore diameter for a commercial MRI scanner is 60 or 70 cm for a long bore or short bore, respectively. This width is large enough to accommodate two medium-build adults when lying side-by-side and face-to-face inside the magnet bore. However, inside the bore, the dimensions of the homogeneous static magnetic field B_0 region are only either a 50 × 50 × 50 cm^3 sphere in a long bore or 50 × 50 × 45 cm^3 ellipsoid in a short bore. Because the two homogeneous RF field B_1 regions of the two CP coils need to be inside this sphere or ellipsoid, the maximum diameter of the axial cross-section of the homogeneous sphere or ellipsoid imposes a limitation on the diameter of the CP coils. Trade-off between maximum-allowed head size and the 50 cm limitation in horizontal direction yields the following practical design parameters: the inner diameter of each birdcage is 25.5 cm and the outer diameter of the cylindrical clearance of each birdcage is 28 cm. This design allows two medium-size heads to be comfortably situated inside two birdcages. Partial posterior areas of the occipital lobe may experience strong static magnetic field inhomogeneity in both subjects. In the event of this occurrence, special shimming may be required; fortunately, the visual cortex is not usually of research focus in social cognitive domains.

From a social cognitive perspective, it is essential that the two subjects being scanned can completely see one another's faces. However, this necessity creates conflict between the first and second design goals: complete facial visibility requires a lower number of rungs on the birdcage, which results in a less homogeneous B_1 field. In this version of DHVC, to minimize the number of rungs for full facial visibility, while keeping a sufficient number of rungs to maintain integrity of the homogeneous mode of a volume coil, two four-rung birdcages (13) were used to construct a DHVC. Favorably, part of the decoupling scheme requires that four rungs are laid out as shown in Fig. 1b, where both sides of the CP coils have no blockage by coil rungs.

Decoupling Two CP Volume Coils

Decoupling two side-by-side CP birdcages has not been adequately addressed in previous literature. This is especially the case concerning the use of a birdcage pair for both transmission and reception, in which passive-only decoupling devices are preferred. Obviously, the well-known overlapping and low input impedance preamplifier decoupling schemes for loop array are not applied in this case (14). Other decoupling schemes, such as capacitor (15,16) or inductor (17) decoupling schemes, are not only insufficient to handle a CP coil pair but also too sensitive with different loads. Here, we present a novel and robust decoupling method for two side-by-side identical CP birdcages that not only performs CP field isolation but also is relatively insensitive to coil load. The proposed method is a combination of geometric decoupling and a decoupling interface (12) made from a directional coupler.

First of all, each singular birdcage is rotated around to a unique azimuthal angle, so that one component of its CP magnetic field is aligned with vertical direction, while another component is aligned with horizontal direction. When two such identical birdcages are placed side-by-side symmetrically, they can be treated as two vertical-field Helmholtz coils in parallel and two horizontal-field Helmholtz coils one in series. The transversal component of the combined field, which contains the CP field that corresponds to MR signals, can be decomposed to even-mode vertical field and odd-mode horizontal field (11). The even-mode magnetic fields in both coils are isolated due to the virtual magnetic wall, defined as geometric decoupling. The odd mode magnetic fields in both coils are tightly coupled due to the virtual magnetic short. The following pertains to all nontransversal components of the combined field, which are not related to MR signal: the fields from two vertical-field Helmholtz coils are sufficiently decoupled by the distance between them; the coupling between two horizontal-field Helmholtz coils joins the odd-mode transversal field together, and the coils are decoupled by the decoupling interface. As only odd-mode fields need to be decoupled, the CP coupling is reduced to linear polarized coupling. Because the two odd-mode ports could differ significantly in loading by two different heads, it is required that the chosen decoupling mechanism be relatively immune from such variance. A decoupling interface (12) made from a directional coupler becomes the obvious optimal solution. Note that realization of the decoupling interface with a directional coupler in our approach is different from the approaches in Ref. 12.

Geometric Decoupling for Even-Mode Field

When the homogeneous mode of a single four-rung birdcage is tuned to the MR resonance frequency at 3 T, the longitudinal component of the field is trivial. Thus, the CP field inside of the birdcage can be approximately

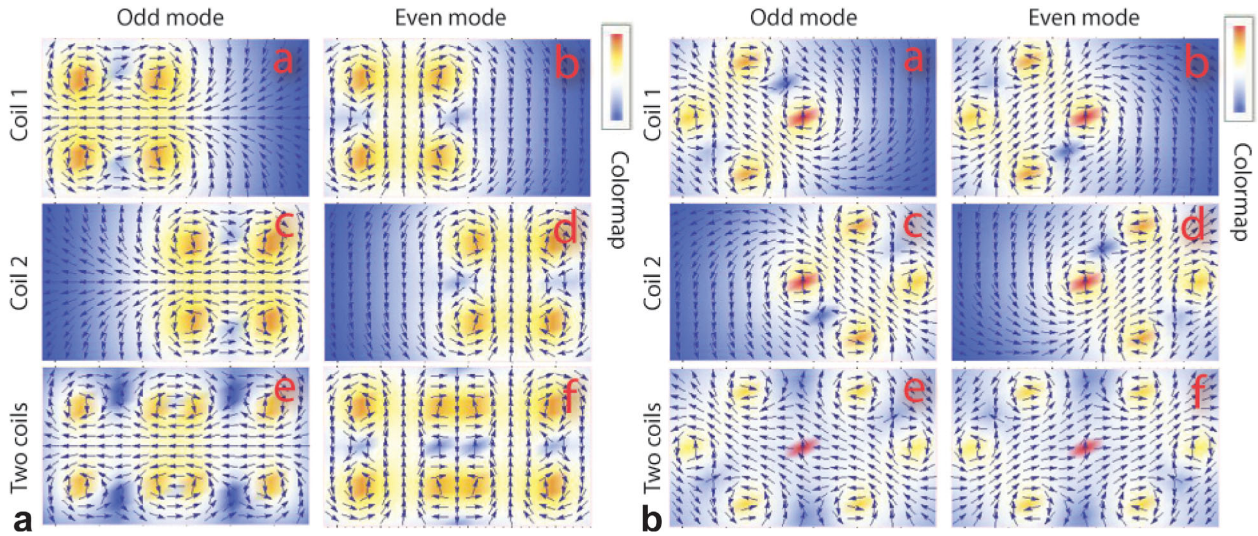

FIG. 2. The left graph Fig. 2**a** shows magnetic field simulation of even- and odd-mode of a DHVC in 45°-setting. Within Fig. 2a, the (a) and (**c**) are the horizontal field components of each birdcage; the (**b**) and (**d**) are the vertical field components. When two birdcages are symmetrically placed side-by-side in the unique orientation described in Fig. 1, the (**e**) is the tightly coupled composite horizontal component and the (**f**) is decoupled composite vertical component. The right graph Fig. 2**b** is the same simulation but for a non-45°-setting, in which decoupled components do not exist.

considered as a transverse electromagnetic field (18). The directions of both quadrature components of the quasi-transverse electromagnetic field depend on azimuthal angles of the four rungs. Only when their angles are at 45°, 135°, 225°, and 315° the quadrature components can be precisely aligned with horizontal and vertical directions, as shown in Fig. 1b and c. This unique Azimuthal angle setting is called "45°-setting." When two identical 45°-setting birdcages are placed side-by-side, each one independently tuned and matched, their fields' vertical components cancel each other at the middle plane that symmetrically separates them. This forms a virtual magnetic wall that isolates two vertical component fields in both birdcages. This type of field isolation is defined as geometric decoupling. The composite field pattern of two vertical field components is called "even-mode," borrowing the concept from a similar situation in two parallel transmission lines. Another part of this concept is "odd-mode," which describes the composite field pattern of two horizontal field components. The even-mode and odd-mode of a dual birdcage pair can be estimated by field simulation based on Biot–Savart Law, as shown in Fig. 2a, which clearly demonstrates the coupling and decoupling behaviors of even and odd modes in a dual birdcage pair. These behaviors have also been verified experimentally. Two identical birdcages are placed side-by-side, as shown in Fig. 1b. Using a loop RF probe to measure vertical and horizontal magnetic field components of the two birdcages, the experimental results confirm that the even-mode is decoupled, indicated by only one trough in their S_{11} measurements, and the odd-mode is tightly coupled, indicated by two distanced troughs in their S_{11} measurements (shown in Fig. 3). Note that two identical non-45°-setting birdcages cannot be decomposed to coupled and decoupled modes. This is illustrated by an example in Fig. 2b, where the Azimuthal angles of four rungs in a birdcage are 0°, 90°, 180°, and 270°.

Thus far, there are no robust methods by which to resolve problems in the CP field of decoupling. However, by intrinsically isolating the two vertical field components, geometric decoupling is transformed from a CP field decoupling problem to a linear polarized field decoupling problem, which can be methodically resolved.

Decoupling Interface for Odd Mode Field

The mechanical structure and electrical loading behavior of the two side-by-side birdcages makes it impossible to achieve decoupling through interconnection of capacitor or inductor on the coils. Thus, an obvious choice for passive decoupling is a decoupling interface (12). Generally, there are many solutions for the decoupling equation in Ref. 12;

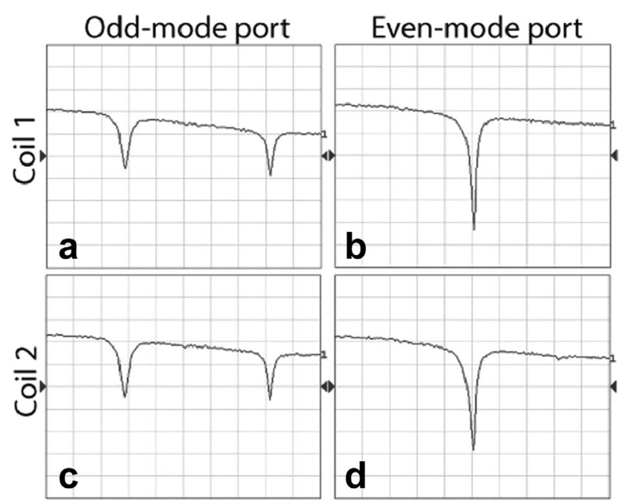

FIG. 3. The S_{11} of the even- and odd-port. (**a**) and (**c**) are the S_{11} of two odd-mode ports, whose split troughs suggest strong coupling. (b) and (**d**) are the S_{11} of two even-mode ports, whose singular trough suggests no coupling.

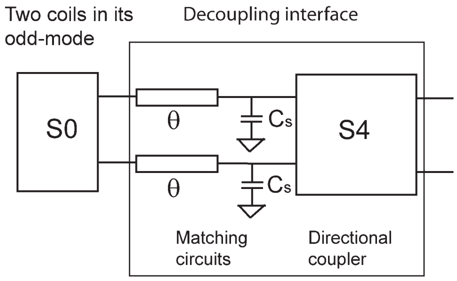

FIG. 4. Diagram of the decoupling interface which consists of two stages: matching circuit and directional coupler.

here, due to its simplistic design and implementation, we selected a four-port directional coupler to serve as the decoupling interface. A directional coupler requires its four ports matched to 50 Ω. However, the odd-mode ports are no longer 50 Ω due to the coupling, and so the first stage in a decoupling interface is the matching, as shown in Fig. 4.

Matching Scheme for Two Coupled Odd-Mode Ports. The two coupled odd-mode ports can be matched by applying transmission lines and shunt capacitors at both odd-mode ports simultaneously (see the matching section in Fig. 4). The design parameters, transmission line length, and shunt capacitance can be determined by following calculation.

First of all, the two odd-mode ports can be treated as a two-port system. When two birdcages are both loaded with human heads, the S-matrix of this mismatched and lossy two-port system can be measured by a network analyzer as,

$$S0 = \begin{pmatrix} S0_{11} & S0_{12} \\ S0_{21} & S0_{22} \end{pmatrix}. \quad [1]$$

The matching scheme is: first, utilizing the two coaxial cables that connect coil's two odd-mode ports and the decoupling interface's two input ports to achieve the desired electrical length θ for the real part of complex impedance matching; then applying the shunt capacitor (C_s) at the directional-coupler end of each cable for the imaginary part of impedance matching. Mathematically, the S-matrix at the ends of the cables, but before shunt capacitors, is

$$\begin{aligned} S1 &= \begin{pmatrix} e^{-j\theta} & 0 \\ 0 & e^{-j\theta} \end{pmatrix} \begin{pmatrix} S0_{11} & S0_{12} \\ S0_{21} & S0_{22} \end{pmatrix} \begin{pmatrix} e^{-j\theta} & 0 \\ 0 & e^{-j\theta} \end{pmatrix} \\ &= \begin{pmatrix} S1_{11} & S1_{12} \\ S1_{21} & S1_{22} \end{pmatrix}. \end{aligned} \quad [2]$$

To calculate the cascade network of this two-port system S_1 and two shunt capacitors, it is convenient to convert Eq. 2 to its corresponding ABCD matrix, which is

$$\begin{pmatrix} A_1 & B_1 \\ C_1 & D_1 \end{pmatrix} = \begin{pmatrix} \frac{(1+S1_{11})(1+S1_{22})+S1_{12}S1_{21}}{2S_{21}} & Z_0\frac{(1+S1_{11})(1+S1_{22})-S1_{12}S1_{21}}{2S_{21}} \\ \frac{1}{Z_0}\frac{(1-S1_{11})(1-S1_{22})-S1_{12}S1_{21}}{2S_{21}} & \frac{(1-S1_{11})(1+S1_{22})+S1_{12}S1_{21}}{2S_{21}} \end{pmatrix}. \quad [3]$$

The Z_0 is characteristic impedance, in this case 50 Ω. The ABCD matrix of a shunt capacitor is

$$\begin{pmatrix} A_c & B_c \\ C_c & D_c \end{pmatrix} = \begin{pmatrix} 1 & 0 \\ j\omega C_S & 1 \end{pmatrix}, \quad [4]$$

Then the ABCD matrix of the matched odd-mode two-port system becomes

$$\begin{pmatrix} A_2 & B_2 \\ C_2 & D_2 \end{pmatrix} = \begin{pmatrix} A_c & B_c \\ C_c & D_c \end{pmatrix} \begin{pmatrix} A_1 & B_1 \\ C_1 & D_1 \end{pmatrix} \begin{pmatrix} A_c & B_c \\ C_c & D_c \end{pmatrix}, \quad [5]$$

which can be transformed back to a S-matrix

$$\begin{aligned} S2 &= \begin{pmatrix} \frac{A_2+B_2/Z_0-C_2Z_0-D_2}{A_2+B_2/Z_0+C_2Z_0+D_2} & \frac{2(A_2D_2-B_2C_2)}{A_2+B_2/Z_0+C_2Z_0+D_2} \\ \frac{2}{A_2+B_2/Z_0+C_2Z_0+D_2} & \frac{-A_2+B_2/Z_0-C_2Z_0+D_2}{A_2+B_2/Z_0+C_2Z_0+D_2} \end{pmatrix} \\ &= \begin{pmatrix} S2_{11} & S2_{12} \\ S2_{21} & S2_{22} \end{pmatrix}. \end{aligned} \quad [6]$$

When matching is achieved, the diagonal terms of S_2 become zero. Thus, the cable length θ and capacitance C_s can be calculated by numerically solving equations

$$\begin{cases} S2_{11} = 0 \\ S2_{22} = 0 \end{cases}. \quad [7]$$

The matched odd-mode ports will significantly simplify the calculation for the directional-coupler style decoupling interface design.

Directional Coupler Design. An arbitrary two-port device can be decoupled by a four-port interface, which satisfied the decoupling Eq. 12. The decoupling equation in Ref. 12 was given in impedance form; its equivalent S-parameter matrix form is given here,

$$S' = \hat{S}_{11} + \hat{S}_{12}(S - \hat{S}_{22})^{-1}\hat{S}_{21}. \quad [8]$$

Here, **S** is the S-matrix of the original arbitrary two-port device, the S-matrix of the four-port decoupling interface is

$$S4 = \begin{pmatrix} S4_{11} & S4_{12} & S4_{13} & S4_{14} \\ S4_{21} & S4_{22} & S4_{23} & S4_{24} \\ S4_{31} & S4_{32} & S4_{33} & S4_{34} \\ S4_{41} & S4_{42} & S4_{43} & S4_{44} \end{pmatrix} = \begin{pmatrix} \hat{S}_{11} & \hat{S}_{12} \\ \hat{S}_{21} & \hat{S}_{22} \end{pmatrix}, \quad [9]$$

and the S-matrix of the final decoupled two ports is S'.

If the two odd-mode ports of the coil are matched at the inputs of directional coupler, as indicated in Eq. 7, then

$$S = \begin{pmatrix} 0 & S2_{12} \\ S2_{21} & 0 \end{pmatrix}. \quad [10]$$

Here, $S2_{12} = S2_{21} = |S2_{12}|e^{j\psi}$ can be either measured by a network analyzer or calculated from $\mathbf{S0}_{12}$ and $\mathbf{S0}_{21}$. Meanwhile, it is well known that the S-matrix of a lossless and matched arbitrary phase four-port directional coupler (11,19) is

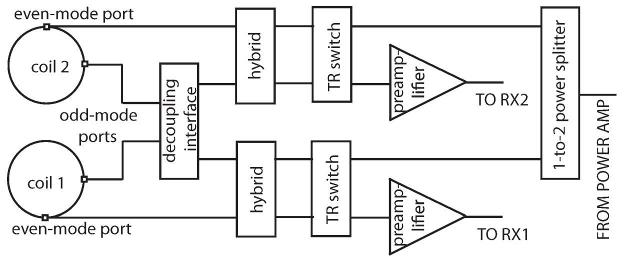

FIG. 5. The block diagram of the RF interface between DHVC and a Siemens MRI scanner. Note that DC paths are not included here. Only RF paths (transmit and receive channels) are displayed here.

$$S4 = \begin{pmatrix} 0 & \alpha & \beta e^{j\varphi} & 0 \\ \alpha & 0 & 0 & \beta e^{j\varphi} \\ \beta e^{j\varphi} & 0 & 0 & \alpha \\ 0 & \beta e^{j\varphi} & \alpha & 0 \end{pmatrix}. \qquad [11]$$

where α and β are real numbers, and φ is the coupler-induced phase shift between the through and coupled signals. By substituting Eqs. 9–11 into the decoupling equation, Eq. 8, the S′ becomes

$$S' = \begin{pmatrix} 0 & \frac{-\alpha+\alpha^2 S2_{12}+\beta^2 e^{j2\varphi} S2_{12}}{-1+\alpha S0_{12}} \\ \frac{-\alpha+\alpha^2 S2_{12}+\beta^2 e^{j2\varphi} S2_{12}}{-1+\alpha S0_{12}} & 0 \end{pmatrix} = \begin{pmatrix} 0 & 0 \\ 0 & 0 \end{pmatrix}. \qquad [12]$$

Here zero in the diagonal terms suggests that the outputs of the decoupling interface are matched, and zero in the cross terms indicates that the two outputs of decoupling interface are decoupled. Assuming that the decoupling interface, **S4**, is passive and lossless, then $\alpha^2 + \beta^2 = 1$, a simple and clean set of solution of Eq. 12 is

$$\alpha = |S2_{12}|, \quad \beta = \sqrt{1-(S2_{12})^2}, \quad \varphi = \tfrac{1}{2}\tan^{-1}\frac{\sin\psi}{\alpha^2-\cos\psi}. \qquad [13]$$

From the Eq. 13, once $S2_{12}$ is known, then α, β, and φ can be calculated, and the design parameters for directional coupler can be fully determined.

An advantage of the directional coupler approach, over other lumped-element network decoupling interfaces, is the fact that its two input ports are mutually isolated. This mutual isolation allows for small coil impedance variations, due to different loads in different coils, to have minimal effects on each other as long as they are close to the matching value. In other words, its decoupling state is a stable state that does not vanish due to small perturbation.

RF/DC Interface Between Coils and Scanner

To integrate the DHVC into a MRI scanner, a RF/DC interface between the coils and the Siemens 3-T MRI scanner is required. The diagram of said interface is shown in Fig. 5. The scanner is configured as 1-channel transmit and 2-channel receive mode. During transmission, once the one-channel transmit signal is fed into the RF/DC interface, it is equally split into two ways by a 1-to-2 power splitter (Werlatone, Patterson, NY). It is then delivered to the two birdcages via two separate TR switches and hybrids (Anaren Microwave, Syracuse, NY), as well as the decoupling interface. During reception, two even-port intrinsically decoupled signals are directly fed into 0° ports on two hybrids. Additionally, two odd-port coupled signals are fed into two input ports of the decoupling interface, and then the two decoupled output signals from the decoupling interface are fed into 90° ports of two hybrids. The two passively decoupled CP signals from two birdcages are delivered to two separate preamplifiers via two separate hybrids and TR switches.

EXPERIMENTS AND RESULTS

Two identical four-rung birdcage volume coils are separately tuned to 123.2 MHz when they are far apart without any coupling. The schematic of the coil as well as its matching circuits is shown in Fig. 6. The diameter of each birdcage is 25.5 cm. Each rung on the birdcage is 21.59 cm long and 2.54 cm wide. To achieve intrinsic geometric decoupling between two side-by-side coils, the Azimuthal angles of four rungs of each birdcage are set at 45°, 135°, 225°, and 315°, assuming 0° is at top of the end-ring. The even and odd ports are placed at 0° and 90° of the end-ring, respectively, see Fig. 1. Both geometric decoupling for the even-mode fields and a decoupling interface for the odd-mode fields are implemented in the DHVC system. A RF/DC interface integrates the DHVC into a Siemens 3-T Skyra MRI scanner (Erlangen, Germany). The DHVC are used for conducting the initial dyadic fMRI studies.

Experimental Verification of the Geometric Decoupling

The two identical birdcage coils are in "45°-setting," the two even-mode ports intrinsically decoupled, as suggested in the Theory and Method section. This phenomenon was directly measured by a network analyzer where $S_{21} = -24$ dB; it was also confirmed by the S_{11} measurements, as shown in Fig. 3b and d, where no resonance trough splitting occurs on either port. On the other hand, the two odd-mode ports become tightly coupled, as shown in Fig. 3a and c, where the S_{11}

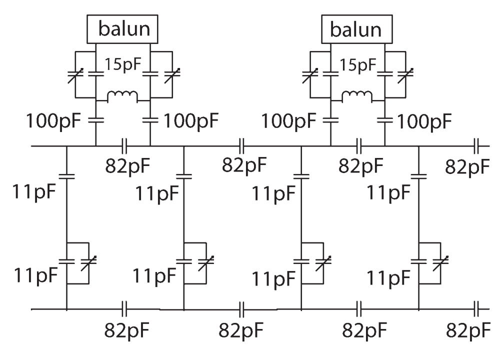

FIG. 6. The schematic of the four-rung birdcage resonator, its matching circuit and balun. A DHVC includes two such birdcages.

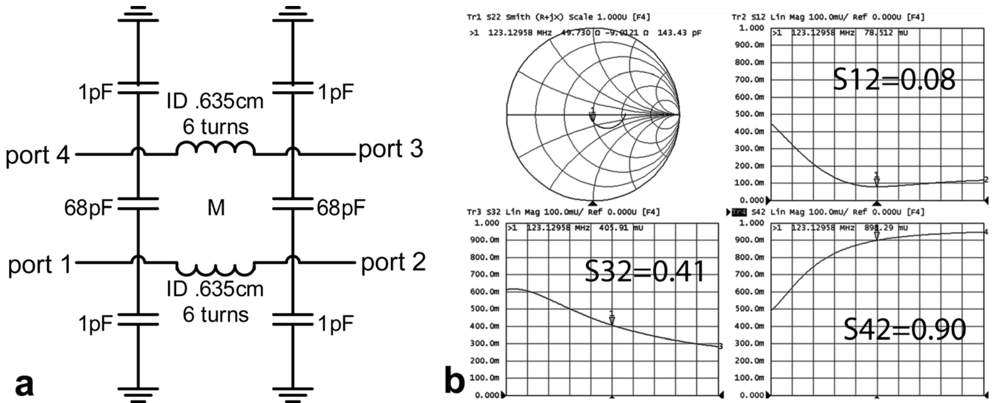

FIG. 7. **a**: Schematic of the designed directional coupler that can decouple two odd-mode ports. Here, ports 1 and 2 are connected to the coils, and ports 3 and 4 are connected to the hybrids. **b**: Performance of the directional coupler in the second stage of the decoupling interface, the S-parameters for given incident power at port 2, where at 123.12 MHz, port 2 is 49 Ω (matched), $S_{12} = 0.08$, $S_{32} = 0.41$, and $S_{42} = 0.90$, which are the precise values designed for decoupled the odd ports of the loaded DHVC.

responses from both ports are largely split into two peaks, a clear sign of strong coupling.

Decoupling Interface Performance

The decoupling interface consists of two stages: matching and decoupling. The directional-coupler has minimal loss and is simpler in design when all four ports are matched. However, due to the strong coupling of horizontal mode, the two odd-mode port impedances significantly deviate from their original 50 Ω. Thus, the first stage of the interface is to match the two odd-mode ports to 50 Ω simultaneously. The second stage is a lumped-element directional-coupler whose coupling precisely compensates the two coils' coupling.

Matching Two Coupled Odd-Mode Ports

Using the procedure for matching two coupled ports as described by Eqs. 1–7 in the Theory and Method section, the cable length and capacitor value are calculated based on the measurements of *S*-parameters of the two odd-mode ports by a network analyzer. The $\mathbf{S0}_{11}$ and $\mathbf{S0}_{22}$ are approximately $0.5 - j0.04$; and the $\mathbf{S0}_{12}$ and $\mathbf{S0}_{21}$ are $\sim 0.02 + j0.04$. Substituting the *S*-parameters into Eq. 1 and solving Eq. 7, we have the electrical length of each coaxial cable at −2.17 rad and the shunt capacitance at 20 pF. Both calculated cable length and shunt capacitance provided first-order estimation for matching. With a slight adjustment to the cable length, and additional assistance of the trimmers, the two coupled odd-mode ports were nicely matched to $49.3 - j6.1$ Ω and $49.7 - j9.0$ Ω by the first stage of the decoupling interface.

Parameter Design for Directional Coupler

The parameter design of an arbitrary phase directional coupler, that can decouple a tightly coupled two port system, is described in Eqs. 10–13. When the two birdcages are loaded with human heads, the coupling measurements of the two matched odd-ports are $|\mathbf{S2}_{21}| = 0.41$ (−7.7 dB) and phase $\psi = 124°$. Thus, plugging in the $\mathbf{S2}_{21}$ values in Eq. 13, the calculated parameters for the directional coupler that can decouple these two odd-ports are $\alpha = 0.41$, $\beta = 0.91$, and $\varphi = 124°$. There are several approaches to build a directional coupler. For the frequency of a 3-T scanner (123.2 MHz), it is easier to implement with lumped elements. In addition, to physically achieve the very strong coupling (0.9) and phase (124°), a unique high pass lumped-element directional coupler was developed specifically for this application, as shown in Fig. 7a. The performance of the directional coupler measured by a network analyzer is shown in Fig. 7b, where all four ports meet all specifications. The robust −50 dB decoupling between two odd ports can be achieved, as shown in Fig. 8, where both coils are loaded with medium size human heads.

Imaging Two People Simultaneously in One Scanner

A prototype DHVC was built and tested on a Siemens Skyra 3-T scanner. The coil installation and two subjects' placement on a MRI scanner are shown in Fig. 9a and b. More than 20 fMRI studies were conducted using this coil system with subject-pairs lying on their sides, face-to-face, inside the magnet bore. The pulse sequence used for the functional studies is EPI with TR = 2000 ms, TE = 30ms, FOV = 500 × 250 mm^2, sampling matrix 128 × 64, slice thickness 4 mm, voxel size 4 × 4 × 4 mm^3, and flip angle 80°. The field map is acquired by GRE sequence with the same resolution and slices as in the functional EPI sequence. The anatomical images are acquired by MPRAGE sequence with voxel size 2 × 2 × 2 mm^3. Each run has 200 measurements in which the subject-pair periodically open and close their eyes, either simultaneously or alternately. Each period has 20 measurements; 10 of them are during open eye intervals and another 10 are during closed eye intervals. The functional data was postprocessed using the fMRI package NEURO3D on the Siemens scanner.

Unlike conventional fMRI in which a well-defined task can be executed in a relatively controlled environment, the outcome of dyadic fMRI is more dynamic and subject-dependent. Thus, new paradigms for its experimental design are required. The experiment described

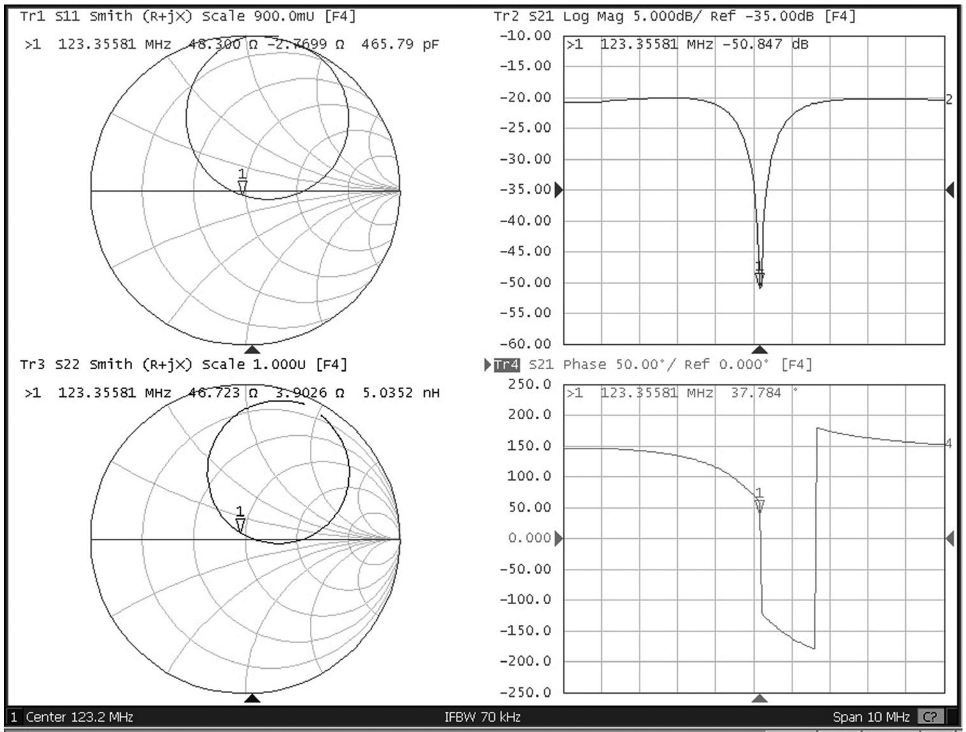

FIG. 8. Performance of the decoupling interface. When the two input ports of the decoupling interface are connected to the −7 dB tightly coupled two odd-mode ports, its two output ports are perfectly matched, as shown in (**a**) and (**b**); the isolation between the two output ports reaches −50 dB, measured by S_{21} between the two ports, (**c**) and (**d**) are the log magnitude and phase of the S_{21}.

here is one of our baseline calibrations, designed to demonstrate the feasibility of the BOLD effect that can be observed using DHVC system setting.

In the study shown in Fig. 10, the two subjects are young and healthy females; their relationship is roommates and friends. They are comfortable and relax with each other in close proximity, and have neither romantic nor defensive feelings toward each other. As illustrated in Fig. 10, the temporal parietal junction, a well-known social cognitive region in fMRI, manifests clear BOLD effects in opening/closing eyes both simultaneously and alternating. Note that a time reversal in the activation/deactivation is manifested: when subjects opened and closed eyes simultaneously, during which the two subjects were instructed to gaze at one another, the BOLD response started noisy, but was becoming more robust at the end; when subject opened and closed eyes alternately, the BOLD response started robustly, but was becoming noisy, as shown in Fig. 10c and d. In other established social cognitive brain regions, like the medial prefrontal cortex, there is activation in the left subject, but not in the right. Furthermore, many regions in the parietal lobe of the right subject show deactivation, which is not replicated in the subject on the left. One strong activation region shared in both subjects is the fusiform face area, which was identified as an area for face recognition.

Our initial experimental data lead us to two basic understandings in dyadic fMRI: first, strong BOLD effects due to interpersonal interaction are clear evidence; second, BOLD activation/deactivation patterns are dynamic and asymmetric between two subjects, due to different personalities and the two subjects' relationship. In this article, our goal is to demonstrate the feasibility that BOLD effect can be observed in this setting experimentally. The second understanding sets the dfMRI apart from the conventional fMRI, and thus requires completely new paradigms in experimental design. These paradigms will be properly and substantially addressed in a separate article.

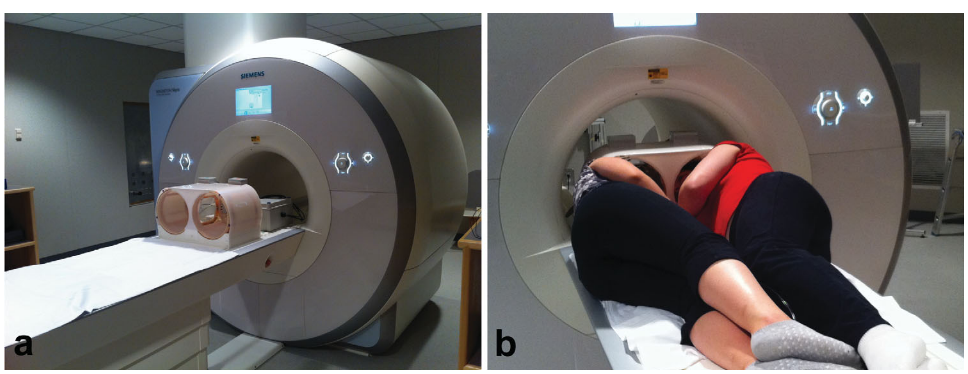

FIG. 9. The (**a**) shows that the DHVC is installed on a Siemens Skyra MRI scanner; the (**b**) demonstrates that two people face-to-face to each other can be scanned simultaneously with the DHVC. [Color figure can be viewed in the online issue, which is available at wileyonlinelibrary.com.]

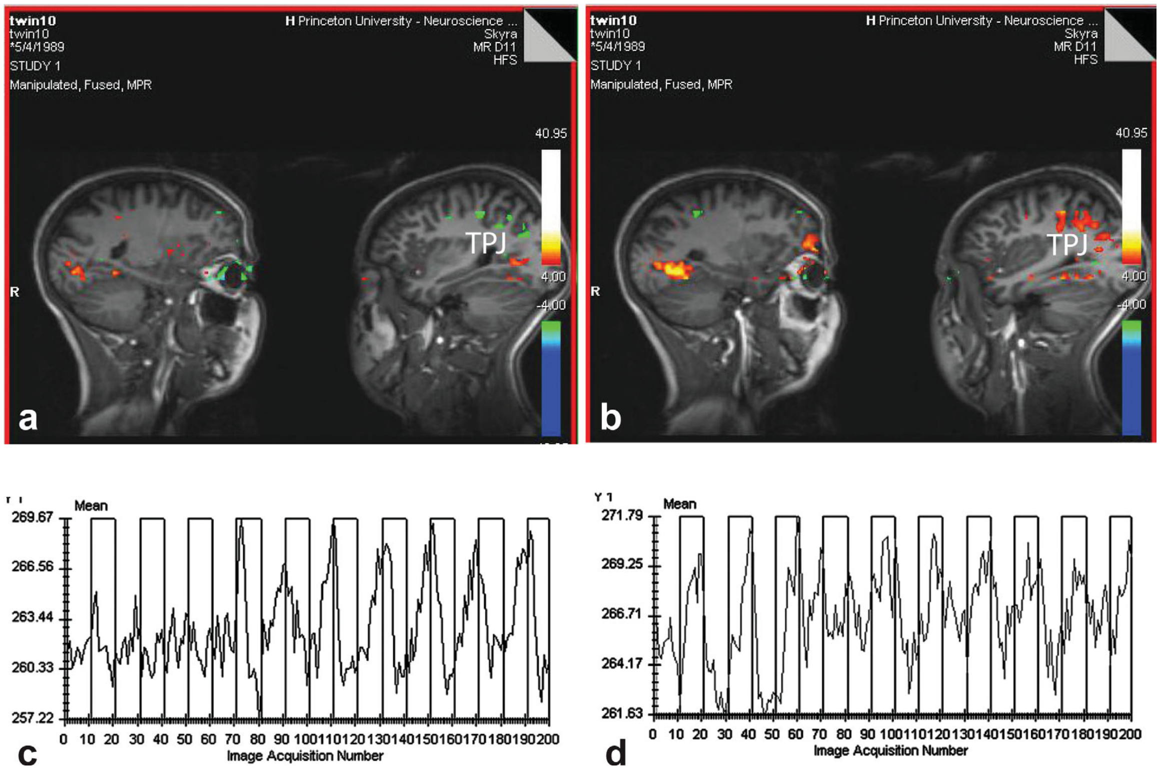

FIG. 10. With DHVC, the BOLD effects of two directly interacting brains were observed for the first time in a dyadic fMRI study between two friends when they were instructed to open and close their eyes, simultaneously (**a**) and alternately (**b**). The (**c**) and (**d**) are the BOLD response time series in temporal parietal junction area during open and close their eyes simultaneously and alternately.

DISCUSSIONS

Trade-off BETWEEN Four- and Eight-Rung Birdcages

It has been well established in the past that the transmit and receive magnetic field homogeneity is less robust for a four-rung birdcage resonator (20). This is also true for DHVC, as shown in Fig. 11a. However, facial expression is a main channel of social communication, and thus the only reason for choosing a four-rung birdcage for dfMRI is to ensure that two subjects have complete view of each others' faces, with 90° clearance between two adjacent rungs. The six- and eight-rung birdcage resonators have also been tested for DHVC. In the case of the six-rung birdcage, 60° clearance between two adjacent rungs could capture a significant portion of facial view and expression. Nevertheless, the restriction on the special orientation of the birdcages for geometric decoupling would require two rungs to be in front of both eyes of each subject, see Fig. 11b, which eliminates the six-rung birdcage as an option for dfMRI. The next possible choice seems to be an eight-rung birdcage. At the special orientation where geometric decoupling is achieved, only one rung is in front of each subject's nose obstructing view. For certain types of studies, if the obstruction can be adapted, an eight-rung birdcage would provide much more robust B_1 field homogeneity, as shown in Fig. 11c. The trade-off between a four- and eight-rung birdcage for dfMRI could be a worthy topic in future, especially after the B_0 shimming for such large field-of-view and two signal sources are significantly improved.

The Issue on Shimming

In a wider and shorter magnet bore, such as Siemens Skyra whose bore diameter is 70 cm and length is 163 cm, the homogeneous static magnetic field defined by the scanner manufacturer is a $50 \times 50 \times 45$ cm^3 ellipsoid. In our experiments, when placing two brains inside this MRI scanner, parts of the occipital lobes of both subjects reach the border of this homogenous field region. The field inhomogeneity can be as much as 3.6 ppm along the border, and rapidly deteriorates beyond this point. This can result in significant SNR reduction, especially for pulse sequences more sensitive to field inhomogeneity, such as EPI for acquiring BOLD effect. During the EPI scan in our current dfMRI studies, the visual cortex area in many medium-size heads are truncated due to the rapid change of field homogeneity in that region. Note that such truncation might not be a serious concern in our current study since the most relevant regions in social interaction fall within the frontal, parietal, and temporal lobes. Ironically, the homogeneous static magnetic field of a narrower and longer magnet bore is slightly larger, a $50 \times 50 \times 50$ cm^3 sphere, as defined by the scanner manufacturer of the Siemens TIM Trio, whose bore diameter is 60 cm and bore length is 198 cm. The field inhomogeneity is also better, about 1.2 ppm along the border, and deteriorates slower than the Skyra does beyond this point. Although the narrower bore has better B_0 performance, it also has a stronger undesired interaction between the DHVC and bore due to their close distance. Additionally, the narrow diameter makes

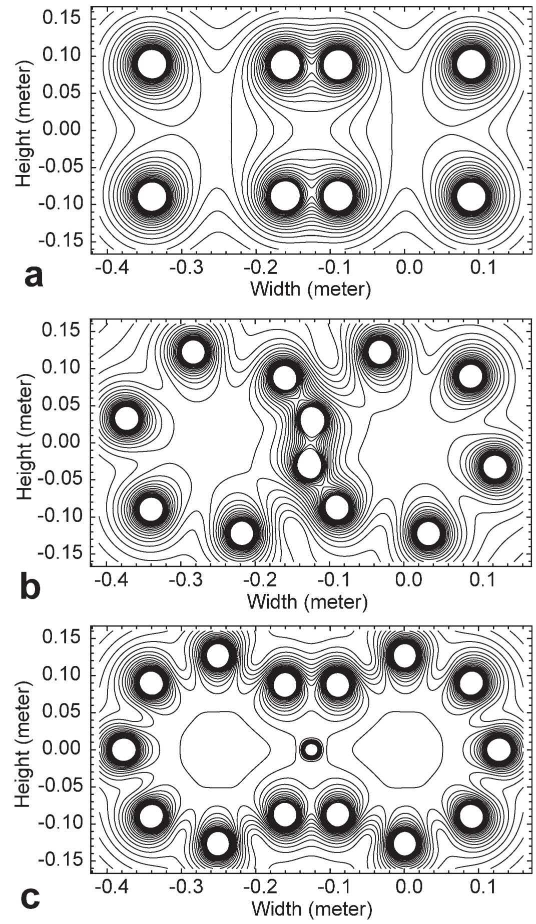

FIG. 11. The B_1 field maps for a (**a**) four-rung, (**b**) six-rung, and (**c**) eight-rung DHVC. All contour lines in the three figures are in the same scale.

it difficult to accommodate two medium-build adults for dfMRI. Further research pertaining to the improvement of shimming on two head areas, but not isocenter regions, in the wider bore are in progress.

Directional Coupler versus Other Circuits for Decoupling Interface

The DHVC loads two head at once. The loadings in each of the two birdcages could be significantly different each time, which could result in a different mismatch at the two odd-mode ports for different subject pairs. This could pose a potential devastating effect on the previous decoupling circuits, such as capacitive or inductive decoupling circuits. Unlike any previously proposed decoupling network, directional coupler has a unique feature that makes it an ideal choice for decoupling the two coils loaded with two different heads. A directional coupler has four ports: through-port, coupled-port, in-port, and isolation-port. As long as the through-port and the coupled port are matched, a different mismatch at the in-port will yield only minimal effects on the isolation-port. In the case of decoupling two odd-ports in DHVC, the through-port and coupled port are connected to the two 0° port on the two hybrids which are matched to 50 Ω. Thus, any mismatch caused by different loading in coil 1 does not greatly affect coil 2, and vice versa. Such isolation between the in-port and the isolation-port is due to balanced phase cancellation at a given frequency; generally, it is immune from a wide range of variations at two input ports, and decoupling is in a stable state. This is not the case for the previously proposed capacitor or inductor decoupling networks, where the two input ports are not isolated from each other. In this case, the decoupling between two varying loadings may not be in a stable state, and a slight variance in the loading between two brains could diminish the decoupling.

CONCLUSIONS

For the first time, a unique DHVC was developed for conducting dyadic fMRI studies for two interacting human brains. It was successfully integrated into a commercial MRI scanner and used for in vivo dual-brain imaging. This opens up a new field for using MRI to directly study social cognition.

On the technical development, the combination of even-odd mode scheme and decoupling interface was proposed and validated for decoupling two strongly coupled CP volume coils, which, unlike surface coils, had not been thoroughly studied prior to this development.

ACKNOWLEDGMENTS

The authors are thankful to Prof. Paul Bottomley at Johns Hopkins University and Prof. John Mugler III, Prof. James Coan, and Karen Hasselmo at University of Virginia for providing the whole-body MRI scanner and subjects for testing before the authors had their own whole-body scanner.

REFERENCES

1. Frith CD, Frith U. Cognitive psychology—interacting minds—a biological basis. Science 1999;286:1692–1695.
2. Saxe R, Kanwisher N. People thinking about thinking people—the role of the temporo-parietal junction in “theory of mind.” Neuroimage 2003;19:1835–1842.
3. Rilling JK, Sanfey AG, Aronson JA, Nystrom LE, Cohen JD. The Neural Correlates of Theory of Mind within Interpersonal Interactions. Neuroimage 2004;22:1694–1703.
4. Amodio DM, Frith CD. Meeting of minds: the medial frontal cortex and social cognition. Nat Rev Neurosci 2006;7:268–277.
5. Stephens G, Silbert L, Hasson U. Speaker-Listener Neural Coupling Underlies Successful Communication. Proc Natl Acad Sci U S A 2010;107(32):14425–14430.
6. Astolfi L, De vico Fallani F, Toppi J, Cincotti F, Wilke C, Yuan H, Doud A, Salinari S, Mattia D, He B, Babiloni F. Imaging the social brain: a simultaneous multi-subject EEG hyperconnetivity study. The 17th annual meeting of Human Brain Mapping, 2011; Quebec City, Canada. p 93.
7. Montague PR, Berns GS, Cohen JD, McClure SM, Pagnoni G, Dhamala M, Wiest MC, Karpov I, King RD, Apple N, Fisher RE. Hyperscanning: simultaneous fMRI during linked social interactions. Neuroimage 2002;16:1159–1164.
8. Redcay E, Dodell-Feder D, Pearrow MJ, Mavros PL, Kleiner M, Gabrieli JD, Saxe R. Live face-to-face interaction during fMRI: a new tool for social cognitive neuroscience. Neuroimage 2010;50:1639–1647.
9. Tropp J. The theory of the bird-cage resonator. J Magn Reson 1989; 82:51–62.
10. Foo TKF, Hayes CE, Kang Y-W. An analytical model for the design of RF resonators for MR body imaging. Magn Reson Med 1991;21:165–177.
11. Rizzi PA. Microwave Engineering Passive Circuits. New Jersey: Prentice Hall; 1988.

12. Lee RF, Giaquinto R, Hardy CJ. Coupling and decoupling theory and its applications to the MRI phased-array. Magn Reson Med 2002;48: 203–213.
13. Murphy-Boesch J, Srinivasan R, Carvajal L, Brown TR. Two Configurations of teh Four-Ring Birdcage Coil for 1H imaging and 1H-Decoupled 31P spectroscopy of teh Human Head. Journal of Magnetic Resonance Series B 1994;103(2):103–114.
14. Roemer PB, Edelstein WA, Hayes CE, Souza SP, Mueller OM. The NMR Phased Array. Magnetic Resonance in Medicine 1990;16(2): 192–225.
15. Wang J. A novel method to reduce the signal coupling of surface coils for MRI. ISMRM 4th annual meeting, 1996; New York. p 1434.
16. Jevtic J. Ladder Networks for Capacitive Decoupling in Phased Array Coils. International Society of Magnetic Resonance in Medicine 9th Scientific Meeting, 2001; Glasgow, Scotland, UK. p 17
17. Lian J, Roemer PB. MRI RF coil. U.S. Pat. 5,804,969, 1998.
18. Vaughan JT, Hetherington HP, Otu JO, Pan JW, Pohost GM. High frequency volume coils for clinical NMR imaging and spectroscopy. Magn Reson Med 1994;32:206–218.
19. Pozar DM. Microwave Engineering. New York: Wiley; 1998.
20. Spence DK, Wright MS. A Method for the Optimization of the Low Pass Birdcage Reonantor with a Finite Number of Legs. The 19th International Conference for IEEE Engineering in Medicine and Biology Society, 1997; Chicago, IL, USA. p 2565.